Research Article

Nasser Amri, Yousef E. Mukhrish, Ismail Özdemir, Nevin Gürbüz, Youssef Arfaoui, Lamjed Mansour, Rafik Gatri, Lotfi Beji, and Naceur Hamdi*

From synthesis to biological impact of palladium bis(benzimidazol-2-ylidene) complexes: Preparation, characterization, and antimicrobial and scavenging activity

https://doi.org/10.1515/mgmc-2023-0007 received March 17, 2023; accepted October 20, 2023

Abstract: Palladium-based complexes with the ligand N-heterocyclic carbene have long received attention as active catalysts for many catalytic reactions. Recently, the biological activities of these air- and moisture-stable complexes have also been investigated. In our work, bis(benzimidazol-2-ylidene)palladium complexes **3a-d** were synthesized by reacting benzimidazolium salts **2a-d** with PdCl₂ under reflux in tetrahydrofuran for 24 h and analyzed by spectroscopy (FT-IR [Fourier transform infrared], ¹H NMR [proton nuclear magnetic resonance]) characterization, ¹³C NMR [carbon-13 (C13) nuclear magnetic resonance]), and elemental analysis. The *in vitro* antibacterial and antifungal activities of these complexes were studied against Gram-positive and Gram-negative microorganisms, and two different fungi showed their remarkable biological

potential. In addition, the analysis of the 2,2-diphenyl-1-picrylhydrazyl (DPPH) free radicals using spectrophotometry showed that they are an antioxidant. The potent antibacterial and antioxidant activities of the synthetic complexes suggest that they are more effective antibacterial agents. Our study extends the biological relevance of palladium bis(benzimidazol-2-ylidene) complexes with antibacterial and antioxidant activities. Furthermore, the main goal of the docking simulation is to provide a detailed analysis of the interaction between the complex and the protein of interest.

Keywords: antimicrobial activity, antioxidant activity, benzimidazolium salts, 2,2-diphenyl-1-picrylhydrazyl, N-heterocyclic carbene, palladium

1 Introduction

N-Heterocyclic carbenes (NHCs) are important supporting ligands (Froese et al., 2017) with their novel biological effects (Janssen-Müller et al., 2017). The steric and electronic properties of NHCs have helped them to be at the forefront of many developments (Azouzi et al., 2018). The NHC and phosphine ligands have played a crucial role in developing organometallic chemistry. These ligand classes, combining two-electron, neutral, and σ-donor, have developed the applications of transition metal complexes (Karthik et al., 2015). Diverse approaches have been made to add a phosphine group to the NHC skeleton in synthesizing organometallic compounds, and metalation has been successfully accomplished through both functionalities. The halide ligand and phosphine molecule used in such complexes are thought to hydrolyze and facilitate the *in vitro* stabilization of complex ions formed by the metal reduction in the metal's coordination sphere. Phosphine-based ligands have widespread pharmacological applications, including antibacterial antioxidant, anticarcinogenic, antiviral, antifungal,

Nasser Amri, Yousef E. Mukhrish: Department of Chemistry, Faculty of Science, Jazan University, P.O. Box 2097, Jazan 45142, Saudi Arabia Ismail Özdemir, Nevin Gürbüz: Catalysis Research and Application Center, İnönü University, 44280 Malatya, Turkey; Department of Chemistry, Faculty of Science and Art, İnönü University, 44280 Malatya, Turkey Youssef Arfaoui: Laboratory of Characterizations, Applications and Modeling of Materials (LR18ES08), Department of Chemistry, Faculty of Sciences, University of Tunis El Manar, Tunis 2092, Tunisia Lamjed Mansour: Zoology Department, College of Science, King Saud

Lamjed Mansour: Zoology Department, College of Science, King Saud University, P.O. Box 2455, Riyadh 11451, Saudi Arabia Pafik Gatri: Laboratoire de Synthèse Organique Sélective et

Rafik Gatri: Laboratoire de Synthèse Organique Sélective et Hétérocyclique Évaluation Biologique LR17ES01 Faculté des Sciences de Tunis, Faculté des Sciences de Tunis Campus Universitaire 1092 Tunis, Université de Tunis El Manar, 1092 Tunis, Tunisia

Lotfi Beji: Department of Physics, College of Sciences and Arts at Arras, Qassim University, Arras, Saudi Arabia

^{*} Corresponding author: Naceur Hamdi, Research Laboratory of Environmental Sciences and Technologies (LR16ES09), Higher Institute of Environmental Sciences and Technology, University of Carthage, Hammam-Lif, Tunisia, e-mail: naceur.hamdi@isste.rnu.tn, tel: +21698503980

and antitumor. It has been recorded that especially phosphinebased nickel(II) and palladium(II) complexes have important bioactivities. These metal-based complexes are used as valuable anticancer drugs due to their effects such as inhibiting cell division and controlling gene expression. The problem with these complexes is that they decompose into highly reactive species in solution, so they do not reach their pharmacological targets such as deoxyribonucleic acid. However, this can be avoided by stabilizing the nickel(II) and palladium(II) complexes with bulky ligands such as triphenylphosphine. In 2006, Organ et al. reported a class of precatalysts based on Pd(II) containing pyridine-derived ligands (O'Brien et al., 2006). The complexes comprise one NHC, two anions (usually Cl or Br), and stabilizing throw-away pyridine derivative ligands (Bal et al., 2021; Erdemir et al., 2020; Lu et al., 2021). Recently, new works have been reported on the antimicrobial, anticancer, antileishmanial, antitoxoplasmal, and enzyme inhibition activities of the PEPPSI-type Pd(II)NHC complexes (Dasgin et al., 2021; Türker et al., 2020). Researchers were particularly synthesized palladium(II) nonplatinum metal complexes due to their strong biological activity and better lipophilicity or solubility than cisplatin (Díez-González and Nolan, 2007; Kumar et al., 2021). Due to its structural similarities to platinum and its potential in vitro cytotoxicity, palladium metal is an excellent metallodrug option (Dindar et al., 2022; Hahn et al., 2005). It has been researched and documented elsewhere that the antiviral, antibacterial, and antifungal activity of Pd(II) complexes with various types of ligands was extensively studied by Garoufis et al. (sulfur and nitrogen donor ligands, Schiff base ligands, and different drugs as ligands) (Scattolin et al., 2021; Zhang and Yu, 2020). Other interesting works showing different intensities of palladium complex activity on various species of bacteria and fungi were studied (Blettner et al., 1999; Crozet et al., 2006;

Franzén and Xu, 2005; Jia et al., 2020; Leadbeater, 2005; Moore and Shaughnessy, 2004; Popović et al., 2021; Rufino-Felipe et al., 2021; Shaughnessy, 2006; Villemin et al., 2001; Wierenga et al., 2019). In our last studies, we have published bis(NHC)Pd(II) complexes that are effective catalysts for direct arylation reactions (Boubakri et al., 2019; Slimani et al., 2022). The purpose of this article is to synthesize new palladium(II) complexes and evaluate their impact on a variety of microbes in vitro. The primary focus of this investigation is on the effects of the newly synthesized Pd(II) complexes on various microorganisms, including Gram-positive and Gram-negative bacteria and different fungi. The goal is to overcome microbial infections to some extent. Thus, we synthesized novel Pd(II) complexes containing halo substitutions and analyzed their in vitro antimicrobial, antifungal, and antioxidant activities to achieve the abovementioned objectives. To optimize metal-NHC complexes, we chose the most famous hybrid density functional theory model (B3LYP) functional, which has been shown to be highly effective in our recent research (Hassen et al., 2022). In addition, we utilized Natural Bond Orbital (NBO) analysis (Glendening et al., 2012) to determine the charge populations at specific sites and quantify the charge transfer (CT) that occurred.

2 Results and discussion

2.1 Preparation of benzimidazolium (2a-d) salts

Benzimidazole salts (**2a–d**) were prepared *via* the two-step N-alkylation process, as depicted in Scheme 1. 1*H*-Benzo[*d*]

Scheme 1: General preparation of benzimidazolium salts (2a-d).

imidazole-(4-(tert-butyl)benzyl) (1a) was prepared by refluxing benzimidazole with 1-(bromomethyl)-4-(tert-butyl)benzene in EtOH for 16 h. The benzimidazolium salts (2a-d) were synthesized by quaternization of 1*H*-Benzo[*d*]imidazole-(4-(*tert*-butyl) benzyl) (1a), with the corresponding benzylbromide derivatives for 48 h at 70°C in degassed dimethylformamide (DMF) to produce the respective benzimidazolium salts (2a-d) with yields in the range of 50-89%. The target salts were obtained as white solids. These salts are stable in solid state and solution against air and moisture. The salts are soluble in chlorinated solvents, alcohols, and water. The reaction has been monitored following thin-layer chromatography, and after this time, the formation of salts (2a-d) has been observed for every target compound. The benzimidazolium salts (2a-d) were air- and moisture-stable both in the solid state and in solution. The FTIR spectroscopy, ¹H NMR and ¹³C{1H} NMR spectroscopy, and elemental analysis data of the title compounds confirm the proposed structures. The synthesis of NHC precursors and their respective ligands is described in Scheme 1.

NMR spectra of all the compounds were analyzed in d-CDCl₃. In the ¹H NMR spectra, acidic protons (NCHN) for benzimidazolium salts (**2a-d**) were seen at 11.17, 11.63, 11.64, and 11.58 ppm, respectively, as a characteristic sharp singlet. Aliphatic carbons appeared from 20.7 to 35 ppm, while aromatic carbons were from 113.38 and 152.82 ppm. Whereas methyl protons showed up as singlets between 1.25 and 2.25 ppm, the aromatic protons showed up as a multiplet between 6.9 and 7.63 ppm. In the ¹³C{1H} NMR spectra of benzimidazole salts (**2a-d**), the NCHN carbon was detected as typical singlets at 142.95, 163.06, 162.9, and 152.8 ppm, respectively. These values are consistent with related literature (Hu et al., 2004; Doğan et al., 2001;

Ozdemir et al., 2010; Iqbal et al., 2013). In the IR spectra, the ν (C=N) bands for salts (2a-d) were observed at 1,548, 1,672, 1,670, and 1,565 cm⁻¹, respectively.

Bis(benzimidazol-2-ylidene)palladium complexes (3a-d) were prepared by reaction of salts (2a-d) with PdCl₂ in high yields of 75-97% (Scheme 2). The reaction was carried out at reflux in anhydrous tetrahydrofuran (THF) in the presence of potassium carbonate (K₂CO₃) as a base for 24 h. Complex 3 is an air-stable solid, soluble in acetone, chloroform, dichloromethane, DMF, dimethyl sulfoxide (DMSO), ethanol, and acetonitrile but insoluble in hexane, ether, and benzene. The structural characterization of the palladium complex was confirmed by NMR, FT-IR, and elemental analysis techniques. In the ¹H NMR spectra of complexes **3a-3d**, the characteristic down-field signals for the acidic C(2)-H protons of the benzimidazolium salts 2a-d disappeared in the ¹H NMR spectra of palladium complex confirming the formation of the NHC-Pd bonds. In the 13 C NMR spectrum of complexes 3a-3d, characteristic signal of C(2)-carbon of imidazolinium salts **3a-3d** between δ = 142.9–162.9 ppm were completely disappeared, and the characteristic Pd-C (carbene) bond signals of the complexes 3a-3d were observed as singlet. In the ¹³C NMR spectra, the carbene signals of the Pd-PEPPSI-NHC complexes 3a-3e were observed at δ = 180.58, 180.81, 180.87, and 180.83 ppm, respectively. The Fourier-transform infrared spectroscopy of the palladium complexes **3a-3d** unveiled a characteristic ν (CN) band, which was observed at 1,608, 1,610, 1,606, and 1,612 cm⁻¹, respectively. The stretching frequency of v(CN) was lower compared to the salt, which can be attributed to the electron flow from the carbene ligand toward the palladium center, causing a weak C=N bond. Moreover, the data from the elemental analysis of the palladium complexes agreed with the suggested structure.

Scheme 2: Preparation of palladium bis(benzimidazol-2-ylidene) complexes 3a-d.

4 — Nasser Amri et al. DE GRUYTER

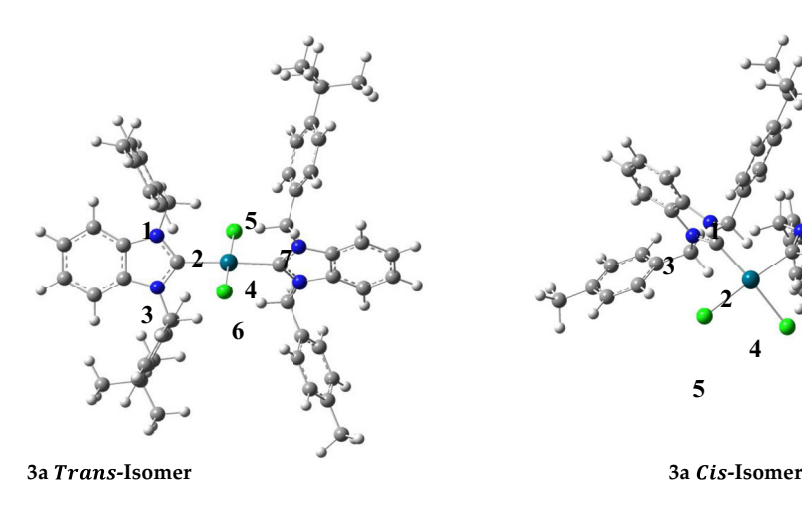


Figure 1: Structures of *trans* and *cis* isomers of complex **3a**.

Numerous attempts were made to obtain a suitable crystal of palladium bis(benzimidazol-2-ylidene) complexes for single-crystal X-ray diffraction study in order to provide a more detailed explanation of the structures of our complexes. The solvent diffusion method was employed using various solvent systems, including dichloromethane/diethyl ether CH₂Cl₂/Et₂O, ethanol/ether EtOH/Et₂O, and others. However, despite all attempts, a suitable single crystal for X-ray analysis could not be obtained for the palladium bis(benzimidazol-2-ylidene) complexes. All spectroscopic and analytical data acquired were consistent with those of previously reported similar palladium complexes of the same type (Slimani et al., 2022).

Both optimized *cis* and *trans* isomer structures of the **3a** complex are shown in Figure 1, taking into account the spin multiplicity of palladium(II). The obtained geometrical parameters are summarized in Table 1. Computed electronic

Table 1: Computed geometric data (bond lengths in Å and bond angle values in °) at the $B_3LYP/6-311$ G(d,p)/LANL2DZ level

	Trans isomer	Cis isomer
	Bond	lengths
N1-C2	1.356	1.358
N3-C2	1.356	1.362
Pd4-C2	2.060	2.029
Pd4-C7	2.390	2.036
Pd4-Cl5	2.390	2.397
Pd4-Cl6	2.061	2.412
	Bond	angles
N1-Pd4-N3	106.8	106.7
C2-Pd4-Cl5	90.0	84.1
C7-Pd4-Cl6	90.0	84.5
CI5-Pd4-CI6	179.9	173.2
C2-Pd4-C7	179.9	171.8
Cl5-Pd4-C7	90.0	93.1
Cl6-Pd4-C2	90.0	99.1

energies relative to the lowest-energy spin multiplicity state S^2 , ΔE (in kcal·mol⁻¹), $\varepsilon_{\text{LUMO}}$, $\varepsilon_{\text{HOMO}}$, and energy gap $\Delta \varepsilon_{\text{L-H}}$ in (eV) of complex **3a** isomers as functions of 2*S* + 1 multiplicities at B3LYP/6-311 G(d,p)/LANL2DZ theory level are summarized in Table 2.

According to the data listed in Table 1, we can conclude that complex $\bf 3a$ crystallizes in square planar geometry. The *trans* isomer for a singlet spin multiplicity is more stable than the *cis* one with relative energy equal to $12.4~\rm kcal\cdot mol^{-1}$. The computed Br5– $\rm Pd4$ –Br6, 2– $\rm Pd4$ –C7, Br6– $\rm Pd4$ –C2, and C7– $\rm Pd4$ –Br5 bond angles in the case of *trans* isomer are equal to 90°. Whereas, in the *cis* isomer, a distorted square planar geometry was found (Table 1). This deformation may be explained by the steric hindrance of aromatic rings.

2.2 Optical property analysis

Complex **3a** showed three absorbance bands at 248 and 288 attributed to π - π * a minor one at 374 nm assigned to the

Table 2: Computed electronic energies relative to the lowest-energy spin multiplicity state S^2 , ΔE (in kcal mol⁻¹), $\varepsilon_{\rm LUMO}$, $\varepsilon_{\rm HOMO}$, and energy gap $\Delta \varepsilon_{\rm LH}$ in eV of complex **3a** isomers as a function of spin 2S+1 at the B3LYP/6-311 G(d,p)/LANL2DZ theory level

Isomer 3a	28 + 1	S^2	ΔΕ	$arepsilon_{ m LUMO}$	$\varepsilon_{ m HOMO}$	$\Delta arepsilon_{ m LH}$
Trans	1	0 2.006 ^a	0.00 51.02	−1.73 −1.08 ^c	-6.73 -4.41 ^c	4.40 2.74 ^c
Cis	1 3	2.000 ^b 0 2.005 ^a 2.000 ^b	12.35 44.06	-3.83 ^c -1.36 -1.09 ^c -4.18 ^c	-6.41° -5.87 -2.95° -6.09°	2.00° 4.52 1.86° 1.91°

 aBefore annihilation. bAfter annihilation. cWhen there are two lines, the first corresponds to α molecular orbital and the second to β molecular orbital.

5

metal-ligand CT (MLCT). The assignment provided is supported by our previous study (Slimani et al., 2022) on a similar PdCl₂-NHC complex, where we examined the performance of three functionals (M06-2X, WB97X-d, and B3LYP). In that study, we observed that the TD-DFT spectra obtained using these functionals closely matched the experimental spectra. Additionally, the confirmation of the CT band assignment was achieved through excited-state CT calculations (Abumelha et al., 2020; Al-Dawood and Al-Hazmi, 2019; Al-Fahemi et al., 2018, 2020; Arslanoğlu and Hamuryudan, 2007; Bayazeed et al., 2020; Boman and Kaletta, 1957; Edwards and Hahn, 2011: El-Daly et al., 1996: El-Metwaly et al., 2019, 2021: Gaber et al., 2017; Garzon et al., 1987; Gwang-Hyeon et al., 2002; Katouah et al., 2019, 2020; Kelly et al., 2018; Keppler and Rupp, 1986; Li-Hua et al., 2013; Richert et al., 2019; Shinde et al., 1999 and Sigel et al., 2018) (Table 3).

2.2.1 CT analysis

A detailed analysis of the CTs that occur between the palladium and NHC fragment was reported since the UV absorption spectrum showed a MLCT transition. We have considered two main fragments, as shown in Figure 2, and the results are displayed in Table 4. An energy diagram showing the molecular orbital interactions and localizations of frontier molecular orbitals is presented in Figure 3.

To evaluate the CT taking place, an analysis of selected sites was performed using NBO analysis (Esrafili and Hadipour, 2011; Karthikeyan et al., 2011; Kepler et al., 2019). This analysis allowed for the determination of the electronic transitions and the extent of charge redistribution between these specific sites. By utilizing NBO analysis, insights into the nature and magnitude of the CT occurring in the system were obtained, enabling a better understanding of the electronic interactions.

According to the data summarized in Table 2, for carbine. This unit is the most efficient donor fragment because it has the highest charge transfer q_{CT} value. Accordingly, the organic moiety (C₂₆H₂₈N₂) is the donor, while the PdCl₂ moiety is the acceptor. An important CT amount occurred from carbene to Pd(II) was obtained. This transferred charge amount was mostly attracted by both chlorides since the latters exhibit strong electron affinity. The CT was confirmed by second-order perturbation theory analysis of the Fock matrix on an NBO basis, as shown in Table 5. The larger the E(2) value, the more intensive the interaction between electron donors and electron acceptors, i.e., the more the donating tendency from electron donors to electron acceptors, the greater the extent of conjugation of the whole system (Sebastian and Sundaraganesan, 2010). The significantly higher stabilization energy value E(2) is observed in the case of intramolecular interaction for the

extinction coefficient values (in dm 3 -mol $^{-1}$ -cm $^{-1}$), and fluorescence quantum yield $\Phi_{
m f}$ of ${f 3a}$ in CHCl $_3$

$\Phi_{ m I}$	0.085	
$\varepsilon_{\rm max\ at\ 374\ nm}\ ({ m dm}^3{ m \cdot mol}^{-1}{ m cm}^{-1})$	300	
$\varepsilon_{\rm max~at~288~nm}~({ m dm}^3{ m \cdot}{ m mol}^{-1}{ m cm}^{-1})$	10,000	
£ _{max at 248 nm} (dm³·mol ⁻¹ ·cm ⁻¹)	12,540	
£ _{max at 370nm} (dm³⋅mol ⁻¹ ⋅cm ⁻¹)	304	
λ _{max(Abs)} (nm)	248	
λ _f (nm)	415	
Solvents	CHCl ₃	

Figure 2: Selected fragments in complex (**3a**) (blue: fragment 1 [carbene derivative], red: fragment 2: PCl₂).

Table 4: Computed charge population (before the complexation q_1 , after the complexation q_2) and the amount of the transferred charge ($q_{\rm CT}$) in (e) of selected sites within complex **3a** at B₃LYP/6-311 + G(d,p)/LANL₂DZ level of theory

Site	N1	C2	N3	Pd4	CI5	CI6
q_1	-0.466	0.149	-0.465	-0.037	0.018	0.018
q_2	-0.420	0.366	-0.422	0.070	-0.479	-0.479
q_{CT}	-0.046	-0.217	-0.043	-0.107	0.497	0.497

3a complex, resulting from the orbital overlap between the carbene derivative (organic base) acting as an electron donor and $PdCl_2$ as an electron acceptor (BD (C7–N8) and LP* (Pd4)).

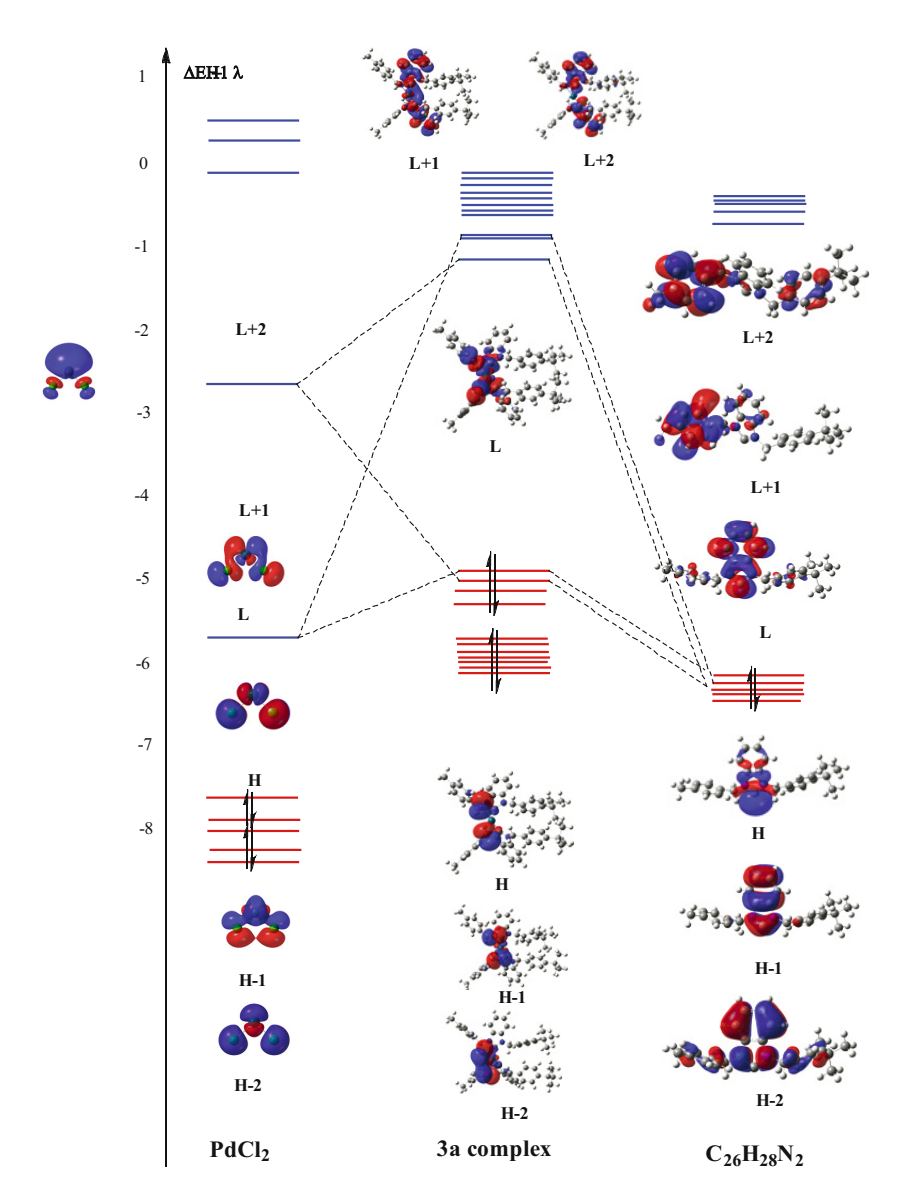


Figure 3: An interaction diagram for complex 3a of symmetry C_1 .

Table 5: Second-order perturbation theory analysis of fock matrix in NBO basis of 3a complex

Donor NBO (<i>i</i>)	Acceptor NBO (j)	<i>E</i> (2) (kcal·mol ^{−1})	<i>E(j)–E(i)</i> (a.u.)	<i>F(i,j)</i> (a.u.)
BD(C7-N8)	LP * (Pd4)	4.51	0.85	0.056
BD (C7-N8)	BD * (Pd4-Cl5)	0.81	0.77	0.023
BD (C7-N8)	BD * (Pd4-Cl6)	1.07	0.36	0.018
BD (C2-N1)	BD * (Pd4-Cl6)	0.71	0.88	0.023
BD (C2-N1)	BD * (Pd4-Cl6)	0.84	0.46	0.018

3 Biological activities

All synthesized benzimidazolium salts (2a-d) and their corresponding palladium bis(benzimidazol-2-ylidene) complexes (3a-d) were tested against two Gram(+) (Micrococcus luteus LB 141107, Listeria monocytogenes ATCC 1911, Staphylococcus aureus ATCC 6538, Bacillus cereus ATCC 14579/Gram (-), and Salmonella typhimurium ATCC 14028). As previously reported, DMSO did not exhibit any antibacterial activity (Shahini et al., 2017; Patil et al., 2010; Gleeson et al., 2008). The antibacterial activities of the NHC precursors (2a-d) and their corresponding palladium bis(benzimidazol-2-ylidene) complexes (3a-d) are listed in Table 1. Compound 3a is more active than compounds **3b** and **3c** against *L. monocytogenes* ATCC 1911, S. aureus ATCC 6538, and S. typhimurium ATCC 14028b. Depending on the type of ligand, the complexes exhibited different levels of antibacterial activity. Palladium bis (benzimidazol-2-ylidene) complexes show increased activity compared to benzimidazolium salts. The complexes showed increased antibacterial activity, which could be explained by the synergistic effect of the complexes to increase lipophilicity. The observed antibacterial activity of these complexes was comparable to our previous palladium bis (benzimidazol-2-ylidene) complexes (Achar et al., 2018). The results obtained are shown in Table 6 and Figure 4.

Table 7 shows that palladium complexes **3a** and **3b** are the most active against *M. luteus* and have a zone of inhibition of 37 mm and a zone of inhibition of 29 mm. Furthermore, Table 6 shows that complex 3a show the high activity against *L. monocytogenes* with a zone of inhibition of 26 mm. Compound **2a** was also shown to be effective against *M. luteus* LB 141107 with a zone of inhibition of 35 mm. *Tetracycline* was used as a benchmark when comparing the results obtained (Kirby and Schmidt, 1997; Sellem et al., 2016). Table 7 shows that the minimum inhibitory concentration (MIC) values of *L. monocytogenes* ATCC 1911 range from 0.1552 to 0.1963 μg·mL⁻¹, and that of *Staphylococcus aureus* ATCC 6538 range from 0.1526 to 1.942 μg·mL⁻¹. From 0.1561 to 0. 4136 μg·mL⁻¹, the values correspond to *S. typhimurium* ATCC 14028.

4 Molecular docking

The docking study was performed using ezCADD (Tao et al., 2019) Smina (Koes et al., 2013) software (https://www.dxulab. org/software). In order to visualize the results, BIOVIA discovery studio 2021 was used (BIOVIA Product Portfolio -BIOVIA - Dassault Systèmes®, n.d.). The salt 2a is an antibacterial activity and can act against Yersinia pestis. The simulation system was built on the crystal structure of PDB ID: 5JQ9 and 2X4M (Zhao et al., 2016), which was downloaded using the Protein Data Bank as a source (https://www.rcsb.org). The protein molecules were purified using pymol (PyMOL | Pymol.Org, n.d.). The downloaded construct is Y. pestis, a determinant of viability or virulence in every bacterial cell tested. Automatic pocket detection was performed using fpocket3 (Schmidtke et al., 2010). Minimum binding affinity (E_b) values (kcal·mol⁻¹) were calculated to evaluate the resulting binding complexes. Molecular docking simulations were performed to predict the best binding configuration of a ligand for its

Table 6: Zones of bacterial inhibition measured in mm for salts 2a-d and their palladium bis(benzimidazol-2-ylidene) complexes 3a-d

Compounds ^a			Microorganis	ms	
	M. luteus LB 141107	L. monocytogenes ATCC 1911	S. aureus ATCC 6538	S. typhimurium ATCC 14028	B. cereus ATCC 14579
2a	35 ± 0.13	23 ± 0.14	23 ± 1.2	24 ± 1.3	22 ± 0.2
2b	24 ± 2.6	22 ± 0.32	22 ± 0.2	23 ± 1.2	21 ± 0.11
2c	22 ± 1.2	22 ± 0.2	21 ± 0.21	22 ± 1.1	20 ± 0.14
2d	21 ± 0.23	21 ± 0.11	20 ± 0.3	21 ± 0.17	20 ± 0.13
3a	37 ± 0.15	26 ± 0.13	25 ± 1.2	26 ± 1.2	25 ± 0.2
3b	29 ± 2.1	24 ± 0.31	24 ± 0.1	24 ± 1.3	24 ± 0.11
3c	27 ± 1.3	23 ± 0.3	22 ± 0.22	23 ± 1.1	22 ± 0.14
3d	24 ± 0.24	22 ± 0.12	21 ± 0.2	22 ± 0.17	21 ± 0.13
Tetracycline			20		

^aZone of bacterial inhibition measured in mm.

8 — Nasser Amri et al. DE GRUYTER

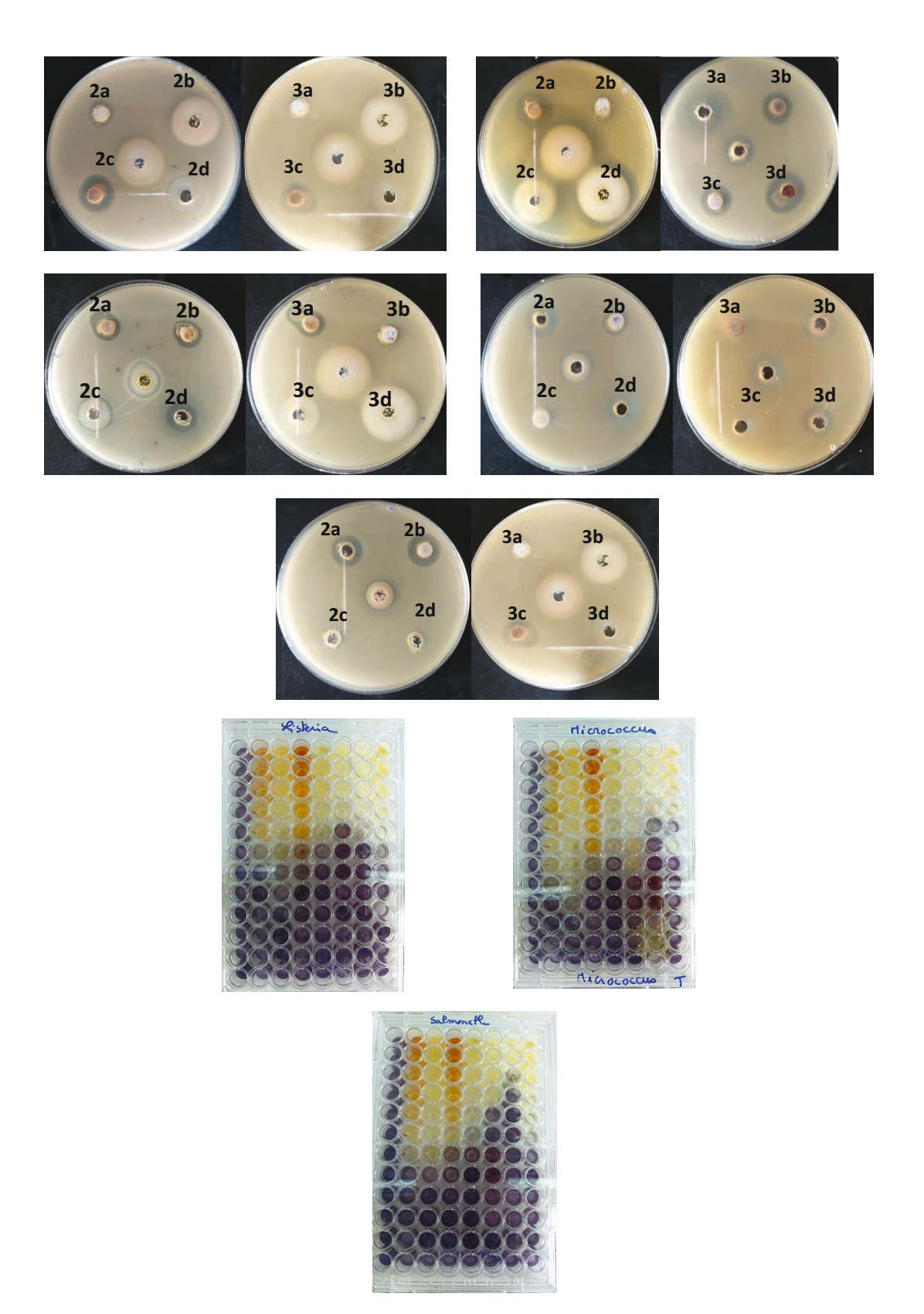


Figure 4: Inhibition zone of ligands and complexes against Gram(+) (*M. luteus* LB 141107, *L. monocytogenes* ATCC 1911, *S. aureus* ATCC 6538, and *B. cereus* ATCC 14579 and Gram(-) (*S. typhimurium* ATCC 14028). Antibacterial activities of salts **2a-d** and their complexes **3a-d** against *M. luteus* LB 141107. Antibacterial activities of salts **2a-d** and their complexes **3a-d** against *S. aureus* ATCC 6538. Antibacterial activities of salts **2a-d** and their complexes **3a-d** against *S. aureus* ATCC 6538. Antibacterial activities of salts **2a-d** and their complexes **3a-d** against *S. aureus* ATCC 6538. Antibacterial activities of salts **2a-d** and their complexes **3a-d** against *S. aureus* ATCC 6538. Antibacterial activities of salts **2a-d** and their complexes **3a-d** against *B. cereus* ATCC 14579. *6a* Method for determining the MIC.

Table 7: MIC of synthesized compounds against *L. monocytogenes* ATCC 1911, *S. aureus* ATCC 6538, and *S. typhimurium* ATCC 14028

Tested compounds (300 µg·mL ⁻¹)	L. monocytogenes ATCC 1911	S. aureus ATCC 6538	S. typhimurium ATCC 14028
2a	0.1763	0.1853	0.1861
2b	0.1863	0.1866	0.1971
2c	0.1963	0.1942	0.3415
2d	0.1846	0.1962	0.4136
3a	0.1552	0.1463	0.1561
3b	0.1562	0.1542	0.1572
3c	0.1643	0.1526	0.3115
3d	0.1654	0.1612	0.3136
Ampicillin	0.002	1.1	1.1

Table 8: An analysis of the crystal structures of Y. pestis proteins 5JQ9 and 2X4M, as well as the predicted binding free energy of the interaction between the salt 2a and the studied proteins (E_b) in (kcal) has been performed

Anti-Y. pestis				
Protein	Resolution	n	Volume	E_{b}
5JQ9	2.10	9	662	-8.0
2X4M	2.55	9	324	-8.1

polymer partner. It creates as many ligand sites as possible at the protein binding site. The best position of the ligand (2a) was chosen based on the best conformation that gave the lowest binding free energy. Table 8 summarizes the crystal structure resolution of the investigated *Y. pestis* protein, the

calculated number of cavities identified, the best protein cavity volume, and the predicted binding free energy of the interaction between salt 2a and the protein. The best positions of the ligand (2a) within the 5JQ9 and 2X4M proteins are indicated in Figures 5 and 6 since it exhibits the lowest free binding energy values -8.0 and -8.1 kcal·mol⁻¹, respectively. The intermolecular interactions between the amino acids and the ligand are also depicted in Figures 4 and 5. In the case of 5JQ9 protein, six types of interactions are revealed: (i) C-H bond with SER; (ii) π -cation with ARG and LYS; (iii) π –σ with PHE; (iv) π – π -shaped with PRO and ARG; (v) alkyl with MET, ILE, and PRO; and (vi) π -alkyl with PRO and ARG. Also, six interactions were observed in the case of 24M: (i) C-H bond with TYR and ASP, (ii) π -anion with GLU, (iii) π - σ with PHE, (iv) π - π -stacked with TYR, (v) alkyl with ILE, and (vi) π -alkyl with ALA. The obtained results allowed us to conclude that the methyl-substituted aromatic ring organic molecule electronic could play a significant role in the biological activity indicated. To investigate the impact of the metal fragment on the biological activity of complex 3a, we utilized the H-Dock server (Yan et al., 2017). The quality of the biological activity was evaluated using the LGscore, which categorizes it as follows: Correct (LGscore > 1.5), Good (3 < LGscore < 5), and Very Good (LGscore > 5). Upon analyzing Table 8, it was observed that complex 3a displayed a very good biological activity with a high LGscore.

Moreover, the data presented in Figure 8 led to the conclusion that the $PdCl_2$ fragment did not interact with the amino acids of *Y. pestis*. Similar to **2a**, complex **3a** exhibited conventional interactions with *Y. pestis* amino acids, including π -donor, π -alkyl, and π -anion interactions.

To investigate the impact of the metal fragment on the biological activity of complex **3a**, we utilized the H-Dock

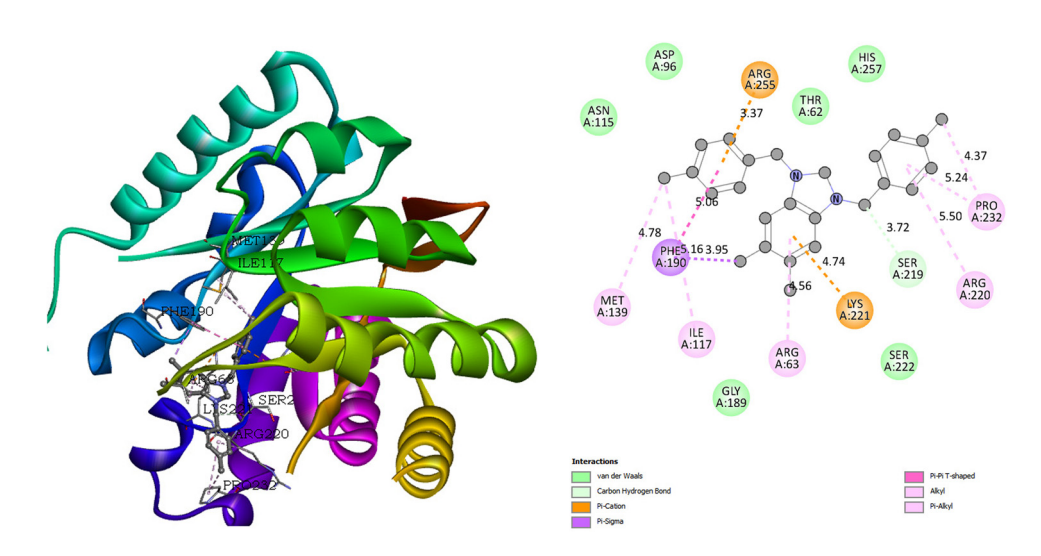


Figure 5: Best position of the salt **2a** within the 5JQ9 (Yersinia pestis) (Left) 2D diagram of the interactions between salt 2a and 5JQ9 (Yersinia pestis) (Right).

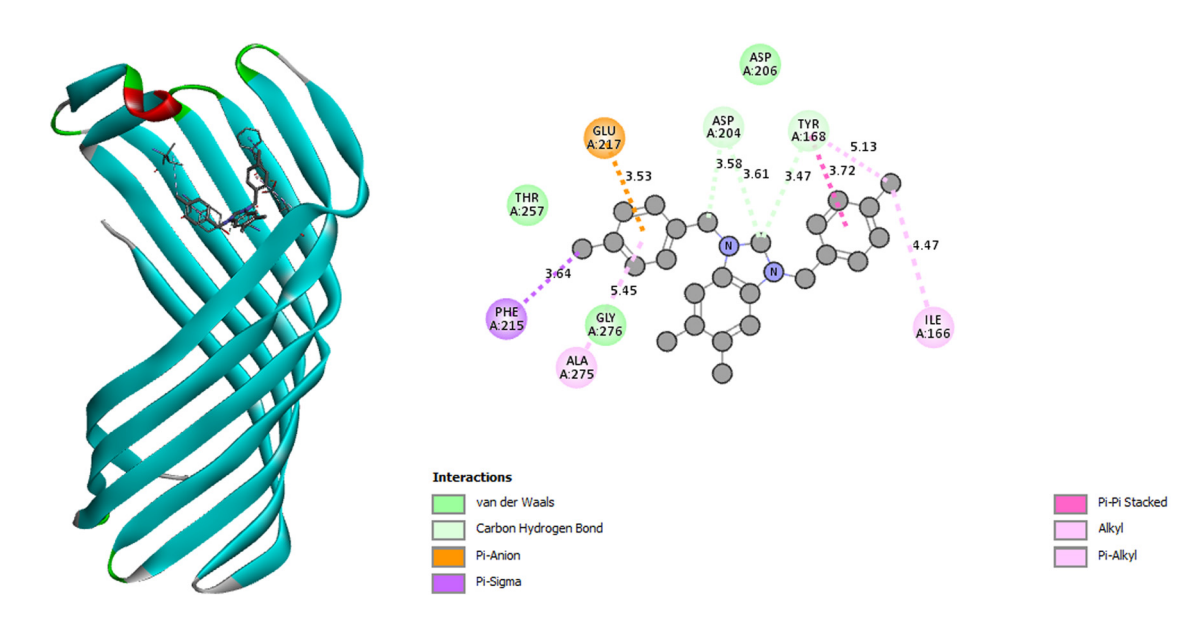


Figure 6: Best position of the salt 2a within the 2X4M (Yersinia pestis) (Left) 2D diagram of the interactions between salt 2a and 2X4M (Yersinia pestis) (Right).

server (Yan et al., 2017). The quality of the biological activity was evaluated using the LGscore, which categorizes it as follows: Correct (LGscore > 1.5), Good (3 < LGscore < 5), and Very Good (LGscore > 5). Upon analyzing Table 7, it was observed that complex **3a** displayed a very good biological activity with a high LGscore.

Moreover, the data presented in Figure 8 led to the conclusion that the $PdCl_2$ fragment did not interact with the amino acids of *Y. pestis*. Similar to **2a**, complex **3a** exhibited conventional interactions with *Y. pestis* amino acids, including π -donor, π -alkyl, and π -anion interactions.

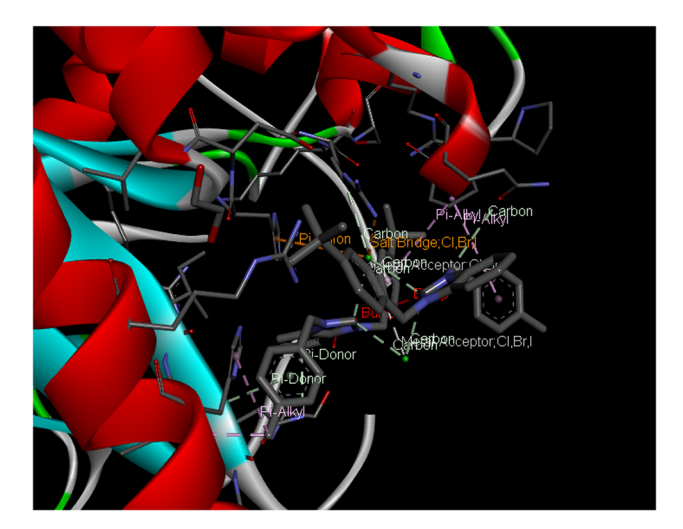


Figure 7: Best position and the interactions of the **3a complex** within the 5|Q9 (Yersinia pestis).

4.1 Antioxidant activity

The scavenging activities have been investigated to support the biological potential of the palladium bis(benzimidazol-2-ylidene) complexes **3a-d** (Jomova et al., 2012; Meyerstein, 2013). The palladium bis(benzimidazol-2-ylidene) complexes **3a-d** were used to examine the decrease in absorbance or scavenging action of a stable-free DPPH (Taha et al., 2011; Trivedi et al., 2012). Comparing the DPPH absorption at 517 nm to the Pd(II) complexes' percentage scavenging activity was done in a concentration-dependent manner (Li et al., 2006; Suh and Chaires, 1995). For Pd(II) complexes, the absorbance of the DPPH free radical at 517 nm with DMSO was 0.906. Complexes have expressed a decrease in absorption (Figure 8).

The IC₅₀ (concentration in grams' mL⁻¹ with 50% effect) was used. Compounds **2d**, **2a**, **3b**, and **3a** from Table 6 show notable DPPH radical scavenging activity. These substances' respective IC₅₀ values were 50.55, 46.88, 47.17, and 48.07 g·mL⁻¹. In terms of ABTS free radical activity, the IC₅₀ of the produced compounds **2a–d** and **3a–d** ranged from 20.45 to 33.17 g·mL⁻¹ (Figure 8). Complexes **3a** (30.22 g·mL⁻¹), **3c** (29.55 g·mL⁻¹), **2d** (33.17 g·mL⁻¹), and **2b** (20.45 g·mL⁻¹ g·mL⁻¹) had the highest activity in the ABTS assay (Figure 7). In the ABTS free radical experiment, the control butylated hydroxytoluene (BHT) (a potent antioxidant molecule) had an IC₅₀ value of g·mL⁻¹ (Figure 8). Due to their antioxidant qualities, Pd compounds have medical and material relevance.

5 Conclusions

This study reports the synthesis of benzimidazolium salts 2a-d and their palladium bis(benzimidazol-2-ylidene) complexes **3a-d**. The structures of these compounds were unambiguously characterized by standard NMR and IR spectroscopy techniques as well as elemental analysis. Palladium bis(NHC) combinations 3(a-d) and benzimidazolium salts 2a-d showed selectivity and moderate activity against a variety of microorganisms. Of particular interest are the results for Gram-positive species that are widespread in the environment. Additionally, these compounds have been shown to scavenge free radicals, suggesting they may have medicinal uses. This has enhanced the penetration of the complexes into the lipid membrane and inhibited the growth of the tested Gram-positive and Gram-negative bacteria. The latter phenomenon demonstrates the widerange activities of the complexes.

Experimental

General methods

All manipulations were carried out under argon using standard Schlenk line techniques in accordance with our earlier work (Slimani et al., 2021). Chemicals and solvents were purchased from Sigma-Aldrich Co. (Poole, Dorset, UK). The solvents used were purified by distillation over the drying agents indicated and were transferred under argon. Melting points were measured in open capillary tubes using

an Electrothermal-9200 melting points apparatus. IR spectra were recorded on an ATR unit in the range of 400–4,000 cm⁻¹ with a Perkin Elmer Spectrum 100 spectrophotometer. ¹H NMR and ¹³C NMR spectra were recorded using Bruker Avance AMX and Bruker Avance III spectrometer operating at 400 MHz (¹H NMR) and 100 MHz (¹³C NMR) in CDCl₃ with TMS added. NMR multiplicities are abbreviated as follows: s = singlet, d = doublet, t = triplet, hept = heptet, and m = multiplet signal. The NMR studies were carried out in high-quality 5 mm NMR tubes. The chemical shifts (d) are reported in ppm relative to CDCl₃. Coupling constants (*J* values) are given in hertz. Elemental analyses were performed by the LECO CHNS-932 elementary chemical analyzer. The chemical shifts (d) are reported in ppm relative to CDCl₃. Coupling constants (*J* values) are given in hertz.

Synthesis of 1-(4-(*tert*-butyl)benzyl)-1*H*-benzo [*d*]imidazole (1a)

This compound was synthesized according to our previous work (Slimani et al., 2022).

1-(4-tert-Butylbenzyl) benzimidazole (1a)

Yield: 100%, m.p. = 120°C, $C_{18}H_{20}N_2$, M = 292 g·mol⁻¹. FT-IR (KBr): $\nu_{(CN)} = 1,716$ (C=N); 1,272 (C-N) cm⁻¹. ¹H NMR (CDCl₃, 400 MHz) δ (ppm) = 8.22 (s, 1H, H₂, NCHN); 7.40–7.42(d, 2H, H_{4',6'}, arom. CH); 5.42 (m, 2H, H_{5,6}, arom. CH); 7.30–7.31 (d, 2H, H_{3',7'}, arom. CH); 7.18 (s, 2H, H_{4,7}, arom. CH); 5.39 (d, 2H,

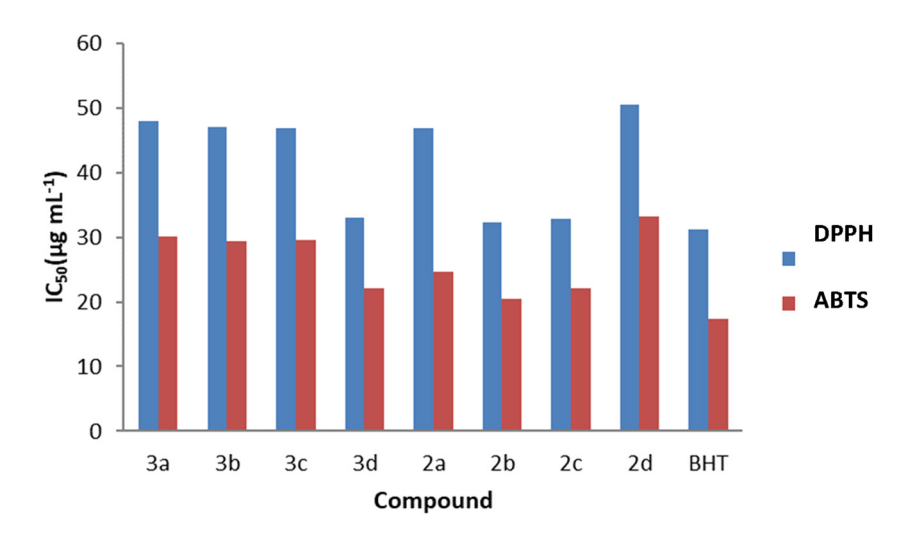


Figure 8: The antioxidative activity of compounds **2a-d** and **3a-d** synthesized was assessed by DPPH and ABTS techniques and expressed as IC_{50} in $g \cdot mL^{-1}$. The BHT was used as a control.

 $H_{1'}$, CH₂); 2.37; 1.23 (s, 9H, $H_{a,b,c}$, 3 × CH₃). ¹³C NMR (CDCl₃, 100 MHz) δ (ppm) = 151.03 (C₂, NCN); 143.28 (C₅, arom. Cq); 142.18 (C₉, arom. Cq); 134.29 (C₂, arom. Cq); 132.25 (C₆, arom. Cq); 130.96 (C₈, arom. Cq); 129.87 (C₅, arom. Cq); 126.93 (C_{4′,6′}, arom. CH); 125.39 (C_{3′,7′}, arom. CH); 119.49 (C₄, arom. CH); 110.57 (C₇, arom. CH); 47.09 (C_{1′}, CH₂); 34.20(C(CH₃)₃, Cq); 31.05 (C_{a,b,c}, 3 × CH₃).

Synthesis of benzimidazolium salts (2a-2d)

The synthesis is carried out by reacting 1.0 g (3.42 mmol) of 1-(4-tert-butylbenzyl) benzimidazole (1a) with an equivalent molar amount of the appropriate aryl bromide or chloride and then dissolving in 2 mL of dried *N,N*-DMF. The solution was stirred at 70°C for 24–48 h. As a result, a product as a white powder was obtained.

1-(4-(*tert*-Butyl)benzyl)-3-(4-methylbenzyl)-2,3-dihydro-1*H*-benzo[*d*]imidazolium bromide (2a)

Yield: 95%, m.p. = 245°C, FT-IR (KBr): ν (CN) (cm⁻¹) = 1,548 (C=N); 1,194 (C-N). ¹H NMR (CDCl₃, 300 MHz) δ (ppm): 11.17 (s, 1H, H₂, NCHN); 7.32 (s, 8H, H_{5,6,4',6',3",4",6",7"}, arom. CH); 7.24 (s, 2H, H_{3',7}, arom. CH); 7.07 (s, 1H, H_{5'}, arom. CH); 6.98 (s, 1H, H_{5''}, arom. CH); 6.91 (s, 2H, H₄, 7, arom. CH); 5.83 (s, 2H, H_{1'}, CH₂); 5.77 (s, 2H, H_{1''}, CH₂); 2.26 (s, 3H, He, CH₃); 2.31 (s, 3H, Ha, CH₃); 2.26 (s, 3H, Hb, CH₃); 2.25 (s, 3H, Hc, CH₃). ¹³C NMR (CDCl₃, 75 MHz) (δ (ppm)): 142.95 (C₂, NCN); 139.42 (C_{2''}, arom. Cq); 137.48 (C_{4',6'}, arom. Cq); 135.58 (C₂, arom. Cq); 134.61 (C_{4'',6''}, arom. Cq); 134.02 (C_{5,6}, arom. Cq); 133.71 (C_{3'',7''}, arom. Cq); 131.08(C₈, 9, arom. Cq); 130.68 (C_{5'}, arom. CH); 128.47 (C_{3',7'}, arom. CH); 125.97 (C_{5''}, arom. CH); 113.79 (C₄, 7, arom. CH); 51.75 (C₁, CH₂); 48.08 (C_{1''}, CH₂); 18.1 (CH₃€); 20.1 C(CH₃)₃; 21.11 (Ca,b, 2 × CH₃); 16.68 (Cc, CH₃). Anal. Calcd for C₂₆H₂₉BrN₂: C, 69.48%; H, 6.50%; N, 6.23%. Found: C, 69.5; H, 76.6; N, 6.23%.

1-(4-(*tert*-Butyl)benzyl)-3-(2,3,5,6-tetramethylbenzyl)-2,3-dihydro-1*H*-benzo[*d*]imidazolium bromide (2b)

Yield: 96%, m.p. = 275°C, FT-IR (KBr): $\nu_{\text{(CN)}}$ (cm⁻¹) = 1,672 (C=N); 1,385 (C–N). ¹H NMR (CDCl₃, 300 MHz) δ (ppm): 11.63 (s, 1H, H₂, NCHN); 7.35 (m, 4H, H_{5,6,5"} arom.); 7.41 (m, 4H, H_{4',6',4",6"}, arom. CH, J_{HH} = 6 Hz); 7.38 (m, 4H, H_{3',7',3",7"}, arom. CH, J_{HH} = 9 Hz); 7.31 (s, 2H, H_{4,7}, arom. CH); 5.74 (s, 4H, H_{1',1"}, 2 × CH₂); 2.94 (s, 3H, H_d, CH₃); 2.87 (s, 3H, H_c, CH₃); 2.26 (s, 9H, H_{a,b}, 3 × CH₃); 2.33 (s, 6H, H_{a,b}, 2 × CH₃). ¹³C NMR (CDCl₃, 75 MHz) (δ (ppm)): 163.06 (C₂, NCN); 152.82 (C_{5',5"}, arom. Cq); 142.31 (C_{2',2"}, arom. Cq); 137.82 (C_{5,6}, arom. Cq); 130.35 (C_{8,9},

arom. Cq); 128.52 ($C_{4',6',4'',6''}$, arom. CH); 126.81 ($C_{3',7',3'',7''}$, arom. CH); 113.80 ($C_{4,7}$, arom. CH); 51.49 ($C_{1',1''}$, 2CH₂); 35.18 (C_{d} , 2CH₃); 31.71 ($C_{a,b}$, 2 × CH₃); 21.23 (C_{c} , CH₃); 27.2 (2CH₃); 29.3 (C(CH₃)₃). Anal. Calcd for $C_{29}H_{35}BrN_2$: C, 70.87%; H, 7.18%; N, 5.70%. Found: C, 70.8; H, 7.2; N, 5.7%.

1,3-Bis(4-(*tert*-butyl)benzyl)-2,3-dihydro-1*H*-benzo[*d*] imidazolium bromide (2c)

Yield: 94%; m.p. = 275°C; FT-IR (KBr): $\nu_{\text{(CN)}}$ (cm⁻¹) = 1,670 (C=N); 1,388 (C–N). ¹H NMR (CDCl₃, 300 MHz) δ (ppm): 11.64 (s, 1H, H₂, NCHN); 7.41 (m, 4H, H_{4,6',4",6"}, arom. CH, J_{HH} = 6 Hz); 7.38 (m, 4H, H_{3',7',3",7"}, arom. CH, J_{HH} = 9 MHz); 7.31 (s, 2H, H_{4,7}, arom. CH); 5.74 (s, 4H, H_{1,1"}, 2 × CH₂); 5.27 (s, 2H, H_{5,6}, arom. CH); 1.25 (s, 12H, H_{a,b,c}, 6 × CH₃). ¹³C NMR (CDCl₃, 75 MHz) (δ (ppm)): 162.9 (C₂, NCN); 152.82 (C_{5',5"}, arom. Cq); 142.31(C_{2',2"}, arom. Cq); 137.82 (C_{5,6}, arom. Cq); 130.35 (C_{8,9}, arom. Cq); 128.52 (C_{4',6',4",6"}, arom. CH); 126.81 (C_{3',7',3",7"}, arom. CH); 113.80 (C4, 7, arom. CH); 51.49 (C1',1", 2CH₂); 20.25 (2 × C((CH₃)₃); 21.23 (C_{a,b,c}, 4 × CH₃). Anal. Calcd for C₂₉H₃₅BrN₂: C, 70.87%; H, 7.18%; N, 5.70%. Found: C, 70.8; H, 7.2; N, 5.7%.

1-(4-(*tert*-Butyl)benzyl)-3-(3,5-dimethylbenzyl)-2,3-dihydro-1*H*-benzo[*d*]imidazolium bromide (2d)

Yield: 92%; m.p. = 235°C; FT-IR (KBr) $v_{(CN)}$ (cm⁻¹): = 1,565 (C=N); 1,359 (C-N) cm⁻¹; ¹H NMR (CDCl₃,300 MHz) δ (ppm): = 11.58 (s, 1H, H₂, NCHN); 7.44 (d, 2H, H_{4'.6'}, arom. CH, $3J_{HH}$ = 7.43 Hz); 7.37 (s, 1H, $H_{5''}$, arom. CH); 7.35 (d, 2H, $H_{3'',7''}$, arom. CH, $3J_{HH}$ = 7.34 Hz); 7.27 (s, 1H, H₃, arom. CH); 5.36 (s, 2H, H_{5,6}, arom. CH); 7.01 (s, 2H, H_{4.7}, arom. CH); 6.94 (s, 1H, H₇, arom. CH); 5.76 (s, 2H, H₁, CH₂); 5.67 (s, 2H, H₁, CH₂); 2.26 (s, 6H, H_{d.e}, $2 \times CH_3$); 1.25 (s, 9H, $H_{a,b,c}$, $3 \times CH_3$). ¹³C NMR (CDCl₃, 75 MHz) $(\delta \text{ (ppm)})$: 152.81 (C₂, NCN); 142.37 (C_{4'.6'}, arom. Cq); 139.59 (C_{2'}, arom. Cq); 137.84 (C_{5"}, arom. CH); 133.11 (C_{2"}, arom. Cq); 131.35 ($C_{5.6}$, arom. Cq); 130.45 ($C_{8.9}$, arom. Cq); 128.53 ($C_{4'',6''}$, arom. CH); 126.77 (C_{3′,5′,7′}, arom. CH); 126.23 (C_{3″,7′′}, arom. CH); 113.82 $(C_{4.7}, arom. CH)$; 51.80 $(C_{1'}, CH_2)$; 51.43 $(C_{1''}, CH_2)$; 35.17 $(C_{d.e}, 2 \times 1)$ CH₃); 31.70 (C_c, CH₃); 21.75 (C_{a,b}, $2 \times \text{CH}_3$); 28.7 (C(CH₃)₃). Anal. Calcd for C₂₇H₃₁BrN₂: C, 69.97%; H, 6.74%; N, 6.04%. Found: C, 70.1; H, 6.8; N, 6.1%.

Synthesis of palladium-bis(NHC) complexes 3(a-d)

The complexes considered in this work are prepared by mixing a solution of 5,6-dimethylbenzimidazolium salts

(1 mmol), $PdCl_2$ (0.5 mmol; 0.09 g), and K_2CO_3 (0.6 g, 4.3 mmol). Next, the anhydrous THF (25 mL) was added, and the mixture was heated at reflux for 24 h at a temperature of about 100°C. The obtained solid was solved in DCM (5 mL) and then purified by flash column chromatography.

Dichlorodi-[1,3-bis-(4-*tert*-butylbenzyl)-5,6-dimethylbenzimidazole-2-ylidene] palladium(II) (3a)

Yield: 94 (%); m.p. 268°C; FT-IR (KBr): $\nu_{\text{(CN)}}(\text{cm}^{-1}) = 1,608; ^{1}\text{H}$ NMR (CDCl₃, 300 MHz) δ (ppm): 7.46 (d, 8H, H_{12,16,19,23,12,16',19',23'}, arom. CH); 7.26 (d, 8H, H_{13,15,20,22,13',15',20',22'}, arom. CH); 6.35 (s, 4H, H_{5,6,5',6'}, arom. CH); 6.83 (s, 4H, H_{4,7,4',7'}, arom. CH); 5.89 (s, 8H, H_{10,17,10',17'}, 4 × CH₂); 1.25 (s, 24H, H_{c,d,e,f,g,h,c',d',e',f'g',h'}, 8 × CH₃). ^{13}C NMR (CDCl₃, 75 MHz) (δ (ppm)): 180.58 (C_{2,2'}, NCN); 150.53 (C_{8,9,8',9'}, arom. Cq); 133.55 (C_{14,21,14',21'}, arom. Cq); 133.01 (C_{11,18,11',18'}, arom. Cq); 131.81 (C_{12,16,19,23,12',16',19',23'}, arom. CH); 127.88 (C_{13,15,20,22,13',15',20',22'}, arom. CH); 125.57 (C_{5,6,5',6'}, arom. Cq); 111.76 (C_{4,7,4',7'}, arom. CH); 52.49 (C_{10,17,10',17'}, 4 × CH₂); 34.63 (C_{d,g,d',g'}, 4 × CH₃); 20.34 (C_{c,e,f,h,c',e',f,h'}, 4 × CH₃); 21.24 (2 × C(CH₃)₃. Anal. Calc. for C₅₂H₅₆Br₂N₄Pd: C, 62.13%; H, 5.82%; N, 5.57%, Found: C, 62.13; H, 5.8; N, 5.6%.

Dichlorodi-[1,3-bis-(4-methylbenzyl)-5,6-dimethylbenzimidazole-2-ylidene] palladium(π) (3b)

Yield: 95 (%); m.p. 266°C; FT-IR (KBr): $\nu_{\text{(CN)}}(\text{cm}^{-1}) = 1,610.$ ¹H NMR (CDCl₃, 300 MHz) δ (ppm): 7.36 (d, 8H, H_{12,16,19,23,12,16',19',23'}, arom. CH); 7.04 (d, 8H, H_{13,15,20,22,13',15',20',22'}, arom. CH); 6.28 (s, 4H, H_{5,6,5',6'}, arom. CH); 6.25 (s, 30H, 10 × CH₃); 6.85 (s, 4H, H_{4,7,4',7'}, arom. CH); 5.91 (s, 8H, H_{10,17,10',17'}, 4 × CH₂); 2.28 (s, 12H, H_{c,d,c',d'}, 4 × CH₃). ¹³C NMR (CDCl₃, 75 MHz) (δ (ppm)): 180.81 (C_{2,2'}, NCN); 137.22 (C_{8,9,8',9'}, arom. Cq); 133.52 (C_{14,21,14',21'}, arom. Cq); 132.99 (C_{11,18,11',18'}, arom. Cq); 131.90 (C_{12,16,19,23,12',16',19',23'}, arom. CH); 129.35 (C_{13,15,20,22,13',15',20',22'}, arom. CH); 127.87 (C_{5,6,5',6'}, arom. Cq); 111.65 (C_{4,7,4',7'}, arom. CH); 52.43 (C_{10,17,10',17'}, 4 × CH₂); 21.30 (C_{c,d,c',d'}, 4 × CH₃); 19.25 (10 (CH₃); 20.24 (2 × C(CH₃)₃. Anal. Calc. for C58H68Br2N4Pd: C, 63.94%; H, 6.48%; N, 5.14%, Found: C, 63.95; H, 6.5; N, 5.2%.

Dichlorodi-bis-[1-(3,5-dimethylbenzyl)-3-(4-methylbenzyl)- 5, 6-dimethylbenzimidazolin-2-ylidene] palladium(π) (3c)

Yield: 97 (%); m.p. 270°C; FT-IR (KBr): $\nu_{(CN)}(cm^{-1}) = 1,606$; ¹H NMR (CDCl₃, 300 MHz) δ (ppm): 7.39 (t, 4H, H_{19,23,19',23'}, arom. CH, J_{HH} = 9 MHz); 7.12 (d, 4H, H_{12,16,12',16'}, arom. CH); 7.06 (t, 4H, H_{20,22,20',22'}, arom. CH, ${}^4J_{HH}$ = 7.5 MHz); 6.89 (m, 4H,

 $H_{4,7,4',7'}$, arom. CH); 6.82(d, 2H, $H_{14,14'}$, arom. CH); 5.92 (s, 2H, H_{10} , CH₂); 2.2 (s, 30H, 10 × CH₃); 5.87 (s, 4H, $H_{17,17'}$, 2 × CH₂); 5.83 (s, 2H, $H_{10'}$, CH₂); 2.29 (s, 6H, $H_{e,e}$, 2 × CH₃); 2.21–2.20 (s, 12H, $H_{c,d,c',d'}$, 4 × CH₃); ¹³C NMR (CDCl₃, 75 MHz) (δ (ppm)): 180.87 (C_{2,2}, NCN); 138.11 (C_{8,9,8',9'}, arom. Cq); 137.22 (C_{13,15,13',15'}, arom. Cq); 135.79 (C_{21,21'}, arom. Cq); 133.64 (C_{11,11'}, arom. Cq); 133.45 (C_{18,18'}, arom. Cq); 133.06 (C_{14,14'}, arom. CH); 131.82 (C_{19,23,19',23'}, arom. CH); 129.26 (C_{20,22,20',22'}, arom. CH); 127.95 (C_{12,16,12',16}, arom. CH); 125.56 (C_{5,6,5',6'}, arom. Cq); 111.64 (C_{4,7,4',7'}, arom. CH); 52.31 (C_{10,17,10',17'}, 4 × CH₂); 21.30 (C_{c,d,c',d'}, 4 × CH₃); 20.37 (C_{e,e'}, 2 × CH₃); 18.28 (10 (CH₃)); 19.26 (4 × C(CH₃)₃). Anal. Calc. for C62H76Br2N4Pd: C, 65.01%; H, 6.86%; N, 4.89%, Found: C, 65.01; H, 6.87; N, 4.9%.

Dichlorodi-bis-[1-(3, 5-dimethylbenzyl)-3-(4-tert-buthylbenzyl)-5,6-dimethylbenzimidazolin-2-ylidene] palladium(π) (3d)

Yield: 75 (%); m.p. 262°C; FT-IR (KBr)): $v_{(CN)}(cm^{-1}) = 1,612$. ¹H NMR (CDCl₃, 300 MHz) δ (ppm): 7.43 (s, 4H, H_{14.14}, arom. CH); 7.38 (s, 4H, H_{19,23,19',23'}, arom. CH); 7.11 (s, 2H, H_{20,22,20',22'}, arom. CH); 6.92 (s, 4H, H_{12,16,12',16'}, arom. CH); 6.85(s, 4H, $H_{4,7,4',7'}$, arom. CH); 6.03 (m, 8H, $H_{10,17,10',17'}$, 4 × CH₂); 2.28 (s, 6H, $H_{f,f}$, 2 × CH₃); 2.17 (s, 12H, $H_{c,d,c',d'}$, 4 × CH₃); 1.30 (s, 12H, $H_{e,g,e',g'}$, 4 × CH₃); 2.12 (s, 12H, 4 × CH₃); ¹³C NMR (CDCl₃, 75 MHz) (δ (ppm)): 180.83 ($C_{2.2}$, NCN); 138.54 ($C_{8.9.8'.9'}$, arom. Cq); 138.12 ($C_{13.15.13'.15'}$, arom. Cq); 135.80 ($C_{21.21'}$, arom. Cq); 134.59 (C_{11,11}', arom. Cq); 133.68 (C_{18,18}', arom. Cq); 132.88 (C_{14.14}', arom. CH); 131.78 (C_{19.23.19'.23'}, arom. CH); 129.96 $(C_{20,22,20',22'}, arom. CH); 127.80 (C_{12,16,12',16'}, arom. CH); 125.58$ (C_{5,6}, 5',6', arom. Cq); 112.02 (C_{4,7,4',7'}, arom. CH); 53.32 (C₁₀, 10', 2 × CH₂); 52.42 (C_{17.17}, 2 × CH₂); 34.73 (C_{c.d.c'.d'}, 4 × CH₃); 31.47 $(C_{f,f}, 2 \times CH_3); 20.36 (C_{e,g,e',g'}, 4 \times CH_3); 19.26 (4 (CH_3); 20.25 (2))$ × C(CH₃)₃. Anal. Calc. for C58H68Br2N4Pd: C, 63.94%; H, 6.48%; N, 5.14%, Found: C, 63.95; H, 6.5; N, 5.14%.

Computational details

The ground state S_0 of the complex was optimized using DFT with hybrid B3LYP (Becke, 1993; Stephens et al., 1994) functional, combined with the 6-311G(d) basis set for the non-metal atoms and a double- ζ quality basis set LANL2DZ (Chiodo et al., 2006) for palladium. Singlet and triplet spin multiplicities were taken into account. Vibrational frequency analyses were performed to confirm that the optimized structures were a true minimum. The electronic populations were analyzed by the NBO population in order to investigate the CT.

The Gaussian16A program package (Gaussian 16, Revision B.01 et al., 2016) was used to perform all calculations. We opted for the B3LYP functional due to its demonstrated effectiveness in optimizing metal-NHC complexes, as established in our recent research (Hassen et al., 2022). NBO analysis (Glendening et al., 2012) was utilized to determine the charge populations at specific sites and subsequently quantify the CT that took place between the relevant fragments in the complex.

The second-order Fock matrix was carried out to evaluate the donor–acceptor interactions in the NBO analysis. The interaction result is a loss of occupancy from the localized NBO of the idealized Lewis structure into an empty non-Lewis orbital. For each donor (i) and acceptor (j), the stabilization energy E(2) associated with the delocalization i-j is estimated as follows (Dindar et al., 2022):

$$E(2) = \Delta_{ij} = q_i F(i, j)^2 / \varepsilon_i - \varepsilon_i$$

UV-Vis electronic absorption spectrum and fluorescence were recorded on a UV-Vis Shimadzu 1650 spectrophotometer, as shown in Figure 9. Quartz cells of 10 mm in length were used. Absorption was measured in the spectrum range of 200–800 nm. The fluorescence spectrum was taken on a Jazco, FP-8200 spectrofluorometer, excitation bandwidth 5 nm, emission bandwidth 5 nm, with an Xe lamp Light source.

Fluorescence quantum yield in liquid was determined using the optically dilute solution relative method with either 9,10-diphenyleanthracene or quinine sulfate solutions, depending on the emission wavelength range. Light intensity was determined using ferrioxalate actinometry (Guven et al., 2017). Eq. 1 was applied to calculate the fluorescence quantum yields:

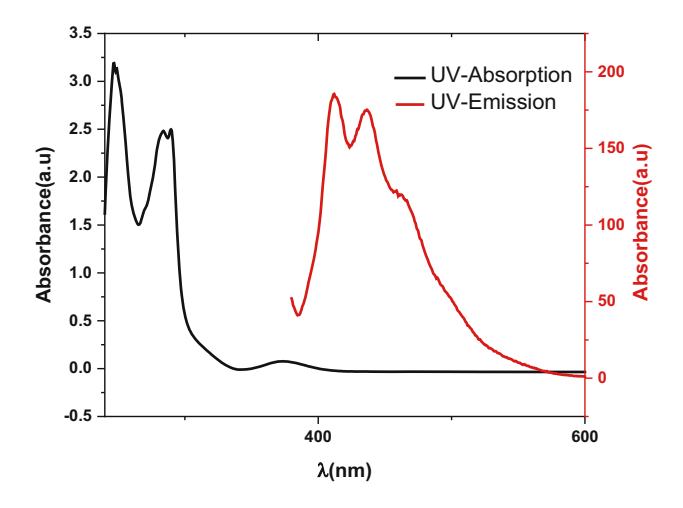


Figure 9: Experimental ultraviolet (UV) absorption and emission ($\lambda_{\rm exc}$ = 370 nm) spectra of 2.5 × 10⁻⁴ M **3a** in CHCl₃.

$$\emptyset_{\rm f}(s) = \emptyset_{\rm f}(r) \times \frac{\int I_{\rm s}}{\int I_{\rm r}} \times \frac{A_{\rm r}}{A_{\rm s}} \times \frac{n_{\rm s}^2}{n_{\rm r}^2}.$$

The integrals denote the corrected fluorescence peak areas, A denotes the absorbance at the excitation wavelength, and n denotes the solvent's refractive index. The subscripts s and r indicate sample and reference, respectively.

Biological activities

Antibacterial activity

Microorganism Test

The biological potential of the synthesized palladium(n) complex was tested against six microorganisms. They studied their antibacterial activity against human pathogenic bacteria, both Gram-negative (*E. coli*; NCIM 2109 and *P. aeruginosa*; NCIM 2036) and Gram-positive (*S. aureus*; NCIM 2079 and *B. subtilis*; NCIM 2250) and two strains of the fungus (*Candida albicans*; NCIM 3471 and *Aspergillus niger*; NCIM 545) by the Kirby–Beurs disc diffusion method using DMSO as solvent on Mueller Hinton agar medium, the concentration is 200 $\mu g \cdot m L^{-1}$. Inhibition zones were measured in millimeters (mm) after incubation for 24 h at 37°C, pH 7.4. The area of inhibition was compared with the standard drugs chloramphenicol (10 μg) and ciprofloxacin (10 μg). Discs containing only DMSO were used as positive controls.

Antioxidant Activities

The antioxidant activity of the stabilized 1-2,5-diphenyl-2-trinitrophenylhydrazine (DPPH) was investigated for its free radical scavenging ability. For this, the complex was mixed with a stock solution of the Pd(II) complex of DPPH (0.002%) in DMSO + water (1:1). To prepare samples, mix DPPH solution with complex solution in a 1:1 ratio, shake vigorously, and incubate for 30 min in the dark. Measure the UV absorbance at 517 nm using a UV/Vis spectrophotometer and observe a decrease in DPPH absorbance, indicating radical scavenging activity, calculated using the following formula:

Purification activity% =
$$(A0 - ASA0) \times 100$$
 (1)

AS is the absorbance of DPPH' with the test compound, and A0 is the absorbance of DPPH' without the test compound. Absorbance data are expressed as the mean \pm standard error of triplicate determinations

Acknowledgments: The authors extended their appreciation to the Researchers Supporting Project number (RSP2023R75), King Saud University, Riyadh, Saudi Arabia.

Funding information: The research was co-funded by the Researchers Supporting Project number (RSP2023R75), King Saud University, Riyadh, Saudi Arabia.

Author contributions: N. A. and Y. E. M. carried out the synthesis, purification, and characterization of the compounds. N. G. and I. O. involved in initial writing the manuscript together with I. O. R. G. carried out the biological experiments. A. Y. carried out the theoretical part. L. B. had substantial contributions to the conception or design of the work, acquisition, analysis, and interpretation of data for the work, drafting the work or revising it critically for important intellectual content, and final approval of the version to be published. N. H. designed and conceived the study and finalized the manuscript. All authors read and approved the final manuscript.

Conflict of interest: Authors state no conflict of interest.

Data availability statement: The datasets generated during and/or analyzed during the current study are available from the corresponding author on reasonable request.

References

- Abumelha H.M., Al-Fahemi J.H., Althagafi I., Bayazeed A.A., Al-Ahmed Z.A., Khedr A.M., et al., Deliberate-Characterization for Ni(II)-Schiff Base Complexes: Promising In Vitro Anticancer Feature that Matched MOE Docking-Approach. J. Inorg. Organomet. Polym. Mater., 2020, 30, 3277-3293.
- Al-Dawood A.Y., Al-Hazmi G.A., Synthesis and characterization for novel Cu(II)-thiazole complexes-dyes and their usage in dyeing cotton to be special bandage for cancerous wounds. J. Mol. Struct., 2019, 1194, 86.
- Al-Fahemi J.H., Khedr A.M., Althagafi I., El-Metwaly N.M., Saad F.A., Katouah H.A., Green synthesis approach for novel benzenesulfonamide nanometer complexes with elaborated spectral, theoretical and biological treatments. Appl. Organomet. Chem., 2018, 32, e4460.
- Al-Fahemi J.H., Khedr A.M., Althagafi I., El-Metwaly N.M., Saad F.A., Katouah H.A., Docking Approach to Predict Inhibition Activity of New Pt(II) Complexes Against Kinase Protein and Human DNA: Full Characterization, HF-FC Modeling and Genotoxicity. J. Inorg. Organomet. Polym. Mater., 2020, 30, 907-922.
- Arslanoğlu Y., Hamuryudan E., Synthesis and derivatization of near-IR absorbing titanylphthalocyanines with dimethylaminoethylsulfanyl substituents. Dyes Pigm., 2007, 75(1), 150-155. Doi: 10.1016/j.dyepig. 2006.05.019.
- Azouzi K., Duhayon C., Benaissa I., Lugan N., Canac Y., Bastin S., et al., Bidentate Iminophosphorane-NHC Ligand Derived from the Imidazo[1,5- α]pyridin-3-ylidene Scaffold. Organometallics., 2018, 37(24), 4726-4735. Doi: 10.1021/acs.organomet.8b00733.
- Bal S., Demirci Ö., Şen B., Taslimi P., Aktaş A., Gök Y., et al., PEPPSI type Pd (II)NHC complexes bearing chloro-/fluorobenzyl group: Synthesis,

- characterization, crystal structures, α-qlycosidase and acetylcholinesterase inhibitory properties. Polyhedron., 2021, 198, 115060. Doi: 10.1016/j.poly.2021.115060.
- Bayazeed A.A., Aljuhani E., Morad M., Abumelha H.M., Bawazeer T.M., Al-Ahmed Z.A., et al., Designed Anticancer Agent from VO(II) Complexes: Spectroscopic Characterization, Structural Optimization, and In Vitro and In Silico Assays towards Breast Cancer, Chem. Select., 2020, 5, 14091-14099.
- Becke A.D., Density-functional thermochemistry. III. The role of exact exchange. J. Chem. Phys., 1993, 98(7), 5648-5652. Doi: 0.1063/1.
- BIOVIA Product Portfolio BIOVIA Dassault Systèmes[®]. 2015. Retrieved June 28, 2022, from https://www.3ds.com/products-services/biovia/ products/.
- Blettner C.G., König W.A., Stenzel W., Schotten T., Microwave-Assisted Agueous Suzuki Cross-Coupling Reactions. J. Org. Chem., 1999, 64(11), 3885-3890. Doi: 10.1021/jo982135h.
- Boman H.G., Kaletta U., Chromatography of rattlesnake venom A separation of three phosphodiesterases. Biochim. Biophys. Acta., 1957, 24, 619-631. Doi: 10.1016/0006-3002(57)90256-1.
- Boubakri L., Chakchouk-Mtibaa A., Al-Ayed A.S., Mansour L., Abutaha N., Harrath A.H., et al., Ru(II)-N-heterocyclic carbene complexes: Synthesis, characterization, transfer hydrogenation reactions and biological determination. RSC Adv., 2019, 9(59), 34406-34420. Doi: 10.1039/C9RA05605J.
- Chiodo S., Russo N., Sicilia E., LANL2DZ basis sets recontracted in the framework of density functional theory. J. Chem. Phys., 2006, 125(10), 104107. Doi: 10.1063/1.2345197.
- Crozet M.D., Castera-Ducros C., Vanelle P., An efficient microwaveassisted Suzuki cross-coupling reaction of imidazo[1,2-a]pyridines in aqueous medium. Tetrahedron Lett., 2006, 47(39), 7061-7065. Doi: 10.1016/j.tetlet.2006.07.098.
- Dasgın S., Gök Y., Barut Celepci D., Taslimi P., İzmirli M., Aktaş A., et al., Synthesis, characterization, crystal structure and bioactivity properties of the benzimidazole-functionalized PEPPSI type of Pd(II)NHC complexes. J. Mol. Struct., 2021, 1228, 129442. Doi: 10.1016/j. molstruc.2020.129442.
- Díez-González S., Nolan S.P., Palladium-catalyzed Reactions Using NHC Ligands. In: F. Glorius (Ed.), N-Heterocyclic Carbenes in Transition Metal Catalysis (Vol. 21, pp. 47-82). Springer, Berlin Heidelberg, 2007. Doi: 10.1007/3418_026.
- Dindar S., Nemati Kharat A., Abbasi A., Green and chemo selective amine methylation using methanol by an organometallic ruthenium complex. J. Organomet. Chem., 2022, 957, 122155. Doi: 10.1016/j. jorganchem.2021.122155.
- Edwards P.G., Hahn F.E., Synthesis and coordination chemistry of macrocyclic ligands featuring NHC donor groups. Dalton Trans., 2011, 40(40), 10278. Doi: 10.1039/c1dt10864f.
- El-Daly S.A., Al-Hazmy S.M., Ebeid E.M., Bhasikuttan A.C., Palit D.K., Sapre A.V., et al., Spectral, Acid-Base, and Laser Characteristics of 1,4-Bis[β-(2-quinolyl)vinyl]benzene (BQVB). J. Phys. Chem., 1996, 100(23), 9732-9737. Doi: 10.1021/jp953083s.
- El-Metwaly N., Althagafi I., Katouah H.A., Al-Fahemi J.H., Bawazeer T.M., Khedr A.M., Synthesis of novel VO(II)-thaizole complexes; spectral, conformational characterization, MOE-docking and genotoxicity. Appl. Organomet. Chem., 2019, 33, e5095.
- El-Metwaly N., Althagafi I., Khedr A.M., Al-Fahemi J.H., Katouah H.A., Hossan A.S., Synthesis and characterization for new Zn(II) complexes and their optimizing fertilization performance in planting corn hybrid. Chem. Pap., 2021, 75, 2121-2133.

- Erdemir F., Aktaş A., Barut Celepci D., Gök Y., New (NHC)Pd(II)(PPh3) complexes: Synthesis, characterization, crystal structure and its application on Sonogashira and Mizoroki–Heck cross-coupling reactions. Chem. Pap., 2020, 74(1), 99–112. Doi: 10.1007/s11696-019-00859-x.
- Franzén R., Xu Y., Review on green chemistry Suzuki cross coupling in aqueous media. Can. J. Chem., 2005, 83(3), 266–272. Doi: 10.1139/v05-048.
- Froese R.D.J., Lombardi C., Pompeo M., Rucker R.P., Organ M.G., Designing Pd–N-Heterocyclic Carbene Complexes for High Reactivity *and* Selectivity for Cross-Coupling Applications. Acc. Chem. Res., 2017, 50(9), 2244–2253. Doi: 10.1021/acs.accounts. 7b00249.
- Gaber M., Khedr A.M., Elsharkawy M., Characterization and thermal studies of nano-synthesized Mn(II), Co(II), Ni(II) and Cu(II) complexes with adipohydrazone ligand as new promising antimicrobial and antitumor agents. Appl. Organomet. Chem., 2017, 31, e3885.
- Garzon F.T., Berger M.R., Keppler B.K., Schmahl D., Comparative antitumor activity of ruthenium derivatives with 5? -deoxy-5-fluorouridine in chemically induced colorectal tumors in SD rats. Cancer. Chemother. Pharmacol., 1987, 19(4):347–9. Doi: 10.1007/BF00261487.
- Gaussian 16, Revision B.01, Frisch M.J., Trucks G.W., Schlegel H.B., Scuseria G.E., Robb M.A., et al., Gaussian, Inc., Wallingford CT, Wallingford, USA, 2016.
- Guven O., Satilmis D., Sonmez F.T., Demir B., Erdogan Ö., Tick Infestation: A 200-Patients' Series. Afr. J. Infect., 2017, 11(2), Article 2. Doi: 10. 21010/ajid.v11i2.8.
- Gwang-Hyeon A., Hak-Won K., Jeong-Ryul K., Soon-Cheol J., Tae-Seop K., Hyun-Tae S., et al., A New Synthetic Process of Lansoprazole. Bull. Korean. Chem. Soc., 2002, 23(4), 626–628. Doi: 10.5012/BKCS.2002. 23.4.626.
- Hahn F.E., Jahnke M.C., Gomez-Benitez V., Morales-Morales D., Pape T., Synthesis and Catalytic Activity of Pincer-Type Bis(benzimidazolin-2ylidene) Palladium Complexes. Organometallics., 2005, 24(26), 6458–6463. Doi: 10.1021/om0507124.
- Janssen-Müller D., Schlepphorst C., Glorius F., Privileged chiral N-heterocyclic carbene ligands for asymmetric transition-metal catalysis. Chem. Soc. Rev., 2017, 46(16), 4845–4854. Doi: 10.1039/C7CS00200A.
- Jia W.-G., Gao L.-L., Wang Z.-B., Wang J.-J., Sheng E.-H., Han Y.-F., NHC-Palladium(II) Mononuclear and Binuclear Complexes Containing Phenylene-Bridged Bis(thione) Ligands: Synthesis, Characterization, and Catalytic Activities. Organometallics., 2020, 39(10), 1790–1798. Doi: 10.1021/acs.organomet.0c00091.
- Jomova K., Baros S., Valko M., Redox active metal-induced oxidative stress in biological systems. Transit. Met. Chem., 2012, 37(2), 127–134. Doi: 10.1007/s11243-012-9583-6.
- Karthik V., Gupta V., Anantharaman G., Synthesis, Structure, and Coordination Chemistry of Phosphine-Functionalized Imidazole/ Imidazolium Salts and Cleavage of a C–P Bond in an NHC–Phosphenium Salt using a Pd(0) Precursor. Organometallics., 2015, 34(15), 3713–3720. Doi: 10.1021/acs.organomet.5b00336.
- Katouah H.A., Al-Fahemi J.H., Elghalban M.G., Saad F.A., Althagafi J.A., El-Metwaly N.M., Practical and computational studies on novel Schiff base complexes derived from green synthesis approach: Conductometry as well as in-vitro screening supported by in-silico study, J. Mol. Liq., 2020, 319, 114116.
- Katouah H.A., Al-Fahemi J.H., Elghalban M.G., Saad F.A., Althagafi J.A., El-Metwaly N.M., et al., Synthesis of new Cu(π)-benzohydrazide nanometer complexes, spectral, modeling, CT-DNA binding with

- potential anti-inflammatory and anti-allergic theoretical features. Mater. Sci. Eng. C., 2019, 96, 740–756.
- Kelly S.A., Pohle S., Wharry S., Mix S., Allen C.C.R., Moody T.S., et al., Application of ω -Transaminases in the Pharmaceutical Industry. Chem. Rev., 2018, 118(1), 349–367.
- Keppler B.K., Rupp W., Antitumor activity of imidazolium-bisimidazole-tetrachlororuthenate(III): A representative of a new class of inorganic antitumor agents. J. Cancer Res. Clin. Oncol., 1986, 111(2), 166–168. Doi: 10.1007/BF00400758.
- Kirby A.J., Schmidt R.J., The antioxidant activity of Chinese herbs for eczema and of placebo herbs—I. J. Ethnopharmacol., 1997, 56(2), 103–108. Doi: 10.1016/S0378-8741(97)01510-9.
- Koes D.R., Baumgartner M.P., Camacho C.J., Lessons Learned in Empirical Scoring with smina from the CSAR 2011 Benchmarking Exercise. J. Chem. Inf. Model., 2013, 53(8), 1893–1904. Doi: 10.1021/ci300604z.
- Kumar S., Dholakiya B.Z., Jangir R., Role of organometallic complexes in olefin polymerization: A review report. J. Organomet. Chem., 2021, 953, 122066. Doi: 10.1016/j.jorganchem.2021.122066.
- Leadbeater N.E., Fast, easy, clean chemistry by using water as a solvent and microwave heating: The Suzuki coupling as an illustration. Chem. Commun., 2005, 23, 2881. Doi: 10.1039/b500952a.
- Li F.-H., Zhao G.-H., Wu H.-X., Lin H., Wu X.-X., Zhu S.-R., et al., Synthesis, characterization and biological activity of lanthanum(III) complexes containing 2-methylene–1,10-phenanthroline units bridged by aliphatic diamines. J. Inorg. Biochem., 2006, 100(1), 36–43. Doi: 10. 1016/j.jinorgbio.2005.09.012.
- Li-Hua Z., Wei-Na W., Yuan W., Guang S., Comment on the section: "Antioxidant measurements and hydroxyl radical scavenging activity" in synthesis, characterization, DNA binding, and antioxidant activities of four copper(II) complexes containing N-(3-hydroxybenzyl)-amino amide ligands. J. Coord. Chem., 2013, 66(12), 2076–2078. Doi: 10.1080/00958972.2013.796511.
- Lu J.F., Zhao J., Sun M., Ji X.H., Huang P., Ge H.G., Synthesis and Crystal Structure of 1-(3-Amino-4-Morpholino-1H-Indazole-1-Carbonyl)-N-(4-Methoxyphenyl)Cyclopropane-1-Carboxamide, a Molecule with Antiproliferative Activity. Crystallogr. Rep., 2021, 66(3), 455–460. Doi: 10.1134/S1063774521030160.
- Moore L.R., Shaughnessy K.H., Efficient Aqueous-Phase Heck and Suzuki Couplings of Aryl Bromides Using Tri(4,6-dimethyl-3- sulfonato-phenyl)phosphine Trisodium Salt (TXPTS). Org. Lett., 2004, 6(2), 225–228. Doi: 10.1021/ol0360288.
- O'Brien C.J., Kantchev E.A.B., Valente C., Hadei N., Chass G.A., Lough A., et al., Easily Prepared Air- and Moisture-Stable Pd–NHC (NHC = N-Heterocyclic Carbene) Complexes: A Reliable, User-Friendly, Highly Active Palladium Precatalyst for the Suzuki–Miyaura Reaction. Chem. Eur. J., 2006, 12(18), 4743–4748. Doi: 10.1002/chem.200600251.
- Popović Z., Smrečki N., Jović O., Mišković Špoljarić K., Gašo-Sokač D., Bušić V., et al., Ternary palladium(II) complexes with N-benzylimi-nodiacetic acid derivatives and 2,2'-bipyridine: Preparation, thermogravimetric, vibrational spectroscopic, DFT, NMR studies and biological activity *in vitro*. Inorg. Chim. Acta., 2021, 516, 120131. Doi: 10.1016/j.ica.2020.120131.
- PyMOL | pymol.org. (n.d.). Retrieved June 28, 2022, from https://pymol.org/2/.
- Richert M., Walczyk M., Cieślak M.J., Kaźmierczak-Barańska J., Królewska-Golińska K., Wrzeszcz G., et al., Synthesis, X-ray structure, physicochemical properties and anticancer activity of *mer* and *fac* Ru(III) triphenylphosphine complexes with a benzothiazole derivative as a co-ligand. Dalton Trans., 2019, 48(28), 10689–10702. Doi: 10.1039/C9DT01803D.

- Rufino-Felipe E., Nayely Osorio-Yáñez R., Vera M., Valdés H., González-Sebastián L., Reyes-Sanchez A., et al., Transition-metal complexes bearing chelating NHC Ligands. Catalytic activity in cross coupling reactions via C H activation. Polyhedron., 2021, 204, 115220. Doi: 10. 1016/j.poly.2021.115220.
- Scattolin T., Piccin A., Mauceri M., Rizzolio F., Demitri N., Canzonieri V., et al., Synthesis, characterization and anticancer activity of palladium allyl complexes bearing benzimidazole-based N-heterocyclic carbene (NHC) ligands. Polyhedron., 2021, 207, 115381. Doi: 10.1016/ j.poly.2021.115381.
- Schmidtke P., Le Guilloux V., Maupetit J., Tuffery P., fpocket: Online tools for protein ensemble pocket detection and tracking. Nucleic Acids Res., 38(Web Server), 2010, W582-W589. Doi: 10.1093/nar/gkg383.
- Sellem I., Kaaniche F., Chakchouk A.M., Mellouli L., Anti-oxidant, antimicrobial and anti-acetylcholinesterase activities of organic extracts from aerial parts of three Tunisian plants and correlation with polyphenols and flavonoids contents. Bangladesh. J. Pharmacol., 2016, 11(2), 531. Doi: 10.3329/bjp.v11i2.26001.
- Shaughnessy K.H., Beyond TPPTS: New Approaches to the Development of Efficient Palladium-Catalyzed Aqueous-Phase Cross-Coupling Reactions. Eur. J. Org. Chem., 2006, 2006(8), 1827-1835. Doi: 10. 1002/ejoc.200500972.
- Shinde U.A., Kulkarni K.R., Phadke A.S., Nair A.M., Mungantiwar A.A., Dikshit V.J., et al., Mast cell stabilizing and lipoxygenase inhibitory activity of Cedrus deodara (Roxb.) Loud. Wood oil. Indian J. Exp. Biol., 1999, 37(3), 258-261. http://nopr.niscpr.res.in/handle/123456789/
- Sigel, A., Sigel, H., Freisinger, E., Sigel, R. K. O. (Eds.), Metallo-Drugs: Development and Action of Anticancer Agents. De Gruyter, Berlin, Boston, 2018. Doi: 10.1515/9783110470734.
- Slimani I., Boubakri L., Özdemir N., Mansour L., Özdemir I., Gürbüz N., et al., Substituted N-heterocyclic carbene PEPPSI-type palladium complexes with different N-coordinated ligands: Involvement in the direct C H bond activation of heteroarenes derivatives with aryl bromide and their antimicrobial, anti-inflammatory and antioxidant activities. Inorg. Chim. Acta., 2022, 532, 120747. Doi: 10.1016/j.ica. 2021.120747.
- Slimani I., Mansour L., Özdemir I., Gürbüz N., Hamdi N., Synthesis, characterization and catalytic activity of PEPPSI-type palladium-NHC complexes. Inorganica Chim. Acta., 2021, 515, 120043. Doi: 10.1016/j.ica.2020.120043.
- Stephens P.J., Devlin F.J., Chabalowski C.F., Frisch M.J., Ab Initio Calculation of Vibrational Absorption and Circular Dichroism

- Spectra Using Density Functional Force Fields. J. Phys. Chem., 1994, 98(45), 11623-11627. Doi: 10.1021/j100096a001.
- Suh D., Chaires J.B., Criteria for the mode of binding of DNA binding agents. Bioorg. Med. Chem., 1995, 3(6), 723-728. Doi: 10.1016/0968-0896(95)00053-J.
- Taha Z.A., Ajlouni A.M., Al Momani W., Al-Ghzawi A.A., Syntheses, characterization, biological activities and photophysical properties of lanthanides complexes with a tetradentate Schiff base ligand. Spectrochim. Acta A Mol. Biomol. Spectrosc., 2011, 81(1), 570-577. Doi: 10.1016/j.saa.2011.06.052.
- Tao A., Huang Y., Shinohara Y., Caylor M.L., Pashikanti S., Xu D., ezCADD: A Rapid 2D/3D Visualization-Enabled Web Modeling Environment for Democratizing Computer-Aided Drug Design. J. Chem. Inf. Model., 2019, 59(1), 18-24, Doi: 10.1021/acs.icim.8b00633.
- Trivedi R., Deepthi S.B., Giribabu L., Sridhar B., Sujitha P., Kumar C.G., et al., Synthesis, Crystal Structure, Electronic Spectroscopy, Electrochemistry and Biological Studies of Ferrocene-Carbohydrate Conjugates. Eur. J. Inorg. Chem., 2012, 2012(13), 2267-2277. Doi: 10. 1002/ejic.201200038.
- Türker F., Noma S.A.A., Aktaş A., Al-Khafaji K., Taşkın Tok T., Ateş B., et al., The (NHC)PdBr2(2-aminopyridine) complexes: Synthesis, characterization, molecular docking study, and inhibitor effects on the human serum carbonic anhydrase and serum bovine xanthine oxidase. Monatsh. Chem., 2020, 151(10), 1557-1567. Doi: 10.1007/ s00706-020-02687-2.
- Villemin D., Gómez-Escalonilla M.J., Saint-Clair J.-F., Palladium-catalysed phenylation of heteroaromatics in water or methylformamide under microwave irradiation. Tetrahedron Lett., 2001, 42(4), 635-637. Doi: 10.1016/S0040-4039(00)02026-8.
- Wierenga T.S., Vanston C.R., Ariafard A., Gardiner M.G., Ho C.C., Accessing Chelating Extended Linker Bis(NHC) Palladium(II) Complexes: Sterically Triggered Divergent Reaction Pathways. Organometallics., 2019, 38(15), 3032-3038. Doi: 10.1021/acs. organomet.9b00356.
- Zhang D., Yu J., Palladium Complexes Bearing Chiral bis(NHC) Chelating Ligands on a Spiro Scaffold: Synthesis, Characterization, and Their Application in the Oxidative Kinetic Resolution of Secondary Alcohols. Organometallics., 2020, 39(4), 605-613. Doi: 10.1021/acs. organomet.9b00833.
- Zhao Y., Shadrick W.R., Wallace M.J., Wu Y., Griffith E.C., Qi J., et al., Pterin-sulfa conjugates as dihydropteroate synthase inhibitors and antibacterial agents. Bioorg. Med. Chem. Lett., 2016, 26(16), 3950-3954. Doi: 10.1016/j.bmcl.2016.07.006.